Journal of Electrotechnology, Electrical Engineering and Management (2026)
Clausius Scientific Press, Canada

DOI: 10.23977/jeeem.2026.090115
ISSN 2560-6697 Vol. 9 Num. 1

Simulation Study on the Gold Wire Bonding Reliability of MEMS Pressure Chips Based on a Detachable Core Package Structure

Xiongkai Dang[1,*], Lijun Yang[1], Shubin Zhang[1], Baolong Su[1], Ziqi Liu[1]

[1]*School of Mechanical and Electrical Engineering, Shaanxi University of Science and Technology, Xi'an, China*

**Corresponding author:18891190199@163.com*

Keywords: MEMS pressure chip; Gold wire bonding; Detachable core package; Finite element simulation; Reliability analysis

Abstract: To address the issues of non-adjustable gold wire bonding height difference, low bonding reliability, and difficulty in chip replacement associated with the planar packaging of MEMS pressure chips in conventional pressure scanning valves, this paper proposes a detachable core-body package structure. By adjusting the PCB thickness to vary the vertical distance between bonding points, the stress and deformation during gold wire bonding are optimized. A circular washer is used as an intermediate support for the pressure chip, which is then secured onto the core-body structural component via a core screw, enabling rapid replacement of individual pressure chips. Using finite element analysis, the equivalent stress and deformation of the gold wire under thermal cycling loads (−40 °C to 125 °C) were evaluated for different bonding point height difference. Results show that the maximum equivalent stress occurs at the neck region of the first bond and increases significantly with increasing vertical separation between the two bonds. The maximum deformation of the bonded wire appears at the midpoint along the wire arc length, and the deformation varies over time. When H12 decreases from 0.6 mm to 0 mm, the peak equivalent stress reduces by 42%, and the wire deformation at high temperature decreases by 33.8%. Life prediction based on the Coffin-Manson model indicates a fatigue cycle life of approximately 1404 cycles under zero height difference bonding, providing theoretical support for highly reliable packaging design in pressure scanning valves.

1. Introduction

Pressure scanning valves are widely employed for multi-point pressure measurements in fields such as wind tunnel testing and aerospace. Currently, the demands for both the quantity and quality of data acquired during pressure sensor research are continuously increasing. Traditional single-channel pressure sensors can no longer satisfy the growing requirements for pressure measurement and are being superseded by highly integrated, high-precision, and highly modular multi-channel pressure scanning valves [1]. A multi-channel pressure scanning valve primarily consists of a pressure sensor assembly and a compact embedded data acquisition system, with the silicon piezoresistive MEMS pressure chip serving as the core sensing element. Packaging technology directly governs the electrical interconnection reliability and long-term stability of the chip. Wire bonding mainly encompasses two forms, namely ball bonding and wedge bonding, and the specific processes include thermocompression bonding, ultrasonic bonding, and thermosonic bonding, among others [2]. Owing to its mature technology and relatively low cost, wire bonding (gold wire bonding) remains one of the prevailing approaches for interconnecting MEMS chips with external circuits. Nevertheless, most existing pressure scanning valves adopt individually packaged MEMS chips, which lead to relatively large volumes and considerable difficulty in replacement when a particular chip fails to meet the required precision or hermeticity. Some studies have proposed directly tiling pressure chips onto a PCB [3] and establishing electrical connections through gold wire bonding; as shown in Figure 1, however, an unadjustable height difference exists between the pressure chip and the PCB, which tends to compromise the reliability of the gold wire bonds. Among the actual failure modes, bonded gold wires frequently experience horizontal wire sweep or vertical wire sagging, where the latter may cause the bonding wire to directly contact the chip edge and result in a short circuit [4].

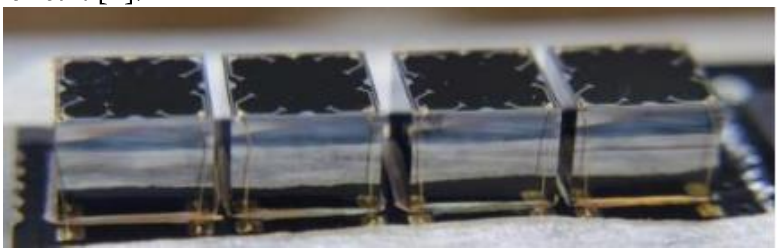

Figure 1: Physical photograph of the planar packaging of the pressure chip.

To address these issues, this paper first proposes a detachable core package structure. By adjusting the thickness of the PCB, the vertical distance between the bonding points is varied, thereby optimizing the stress and deformation of the gold bonding wire. A threaded circular spacer is adopted as an intermediate support for the pressure chip: the pressure chip is bonded onto the circular spacer, and the resulting chip–spacer assembly is secured to the core package structural component using core screws, thus greatly facilitating the replacement of individual pressure chips. Subsequently, finite element simulation is conducted to investigate the influence of different height differences on the equivalent stress and deformation of the gold wire under temperature cycling loads. Finally, the Coffin–Manson empirical formula is applied to perform reliability analysis and lifetime prediction for the Au wire [5].

2. Design of the Detachable Core Package Structure

The detachable core package structure consists as shown in Figure 2, from top to bottom, of a pressure chip, a circular spacer, a PCB, a PT1000 temperature resistor, a core package structural component, a core screw, and a sealing ring. Both the circular spacer and the core package structural component are provided with a threaded pressure inlet hole of 1 mm in diameter, which accurately introduces the external measured pressure into the pressure sensing region of the chip. During the packaging process, a single pressure chip is first bonded onto the circular spacer using a die-attach adhesive. The bonding process must ensure that the inlet hole of the chip is coaxial with that of the spacer and that no adhesive infiltrates the holes. Subsequently, the PCB is fixed onto the core package structural component using the die-attach adhesive during its curing. A through-hole of 1 mm in diameter is formed between the PCB and the structural component, serving as both a reference pressure port and a positioning hole. The PT1000 temperature resistor and the cured pressure chip assembly are then installed in their corresponding positions on the structural component. The pressure chip assembly is secured by the core screw, which features a through-hole of 0.5 mm in diameter in its center for introducing the measured pressure. Gold wire bonding is performed to connect the bonding pads on the temperature resistor and the pressure chip to those on the PCB, thereby achieving electrical interconnection. Finally, a sealing ring is placed into the groove on the back side of the core package, and sealing grease is applied to ensure the hermeticity of the overall pneumatic path.

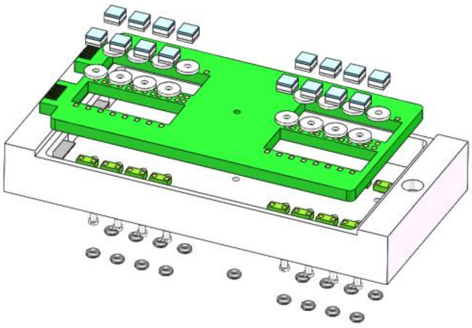

Figure 2: Schematic diagram of the detachable core package structure.

The key feature of this structure lies in the following aspects: the slot width W of the PCB determines the horizontal distance between the two bonding points, while the adjustable thickness of the PCB alters the vertical distance between the top pad of the pressure chip and that of the PCB—namely, the height difference H_{12} between the two bonding points of the gold wire. By varying the thickness of the PCB, this height difference can be adjusted accordingly, thereby providing a structural basis for the subsequent optimization of bonding reliability. Figure 3 shows the physical photograph of the detachable core package.

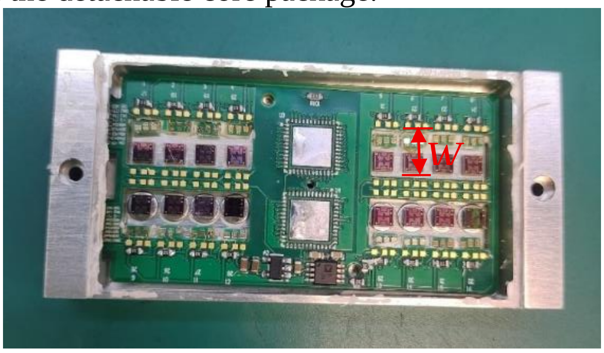

Figure 3: Physical photograph of the detachable core package.

3. Finite Element Simulation of Gold Wire Bonding under Temperature Cycling

3.1. Finite Element Model

The two bonding points are connected by means of gold ball bonding [6]. The structural parameters of the Au wire bond primarily include the horizontal distance L_{12} between bond 1 and bond 2, the vertical distance H_{12} between the two bonds, the loop height h, and the wire diameter D. The present study focuses on the vertical distance H_{12} between the two bonding points of the gold wire.Figure 4 shows the parametric structural model.

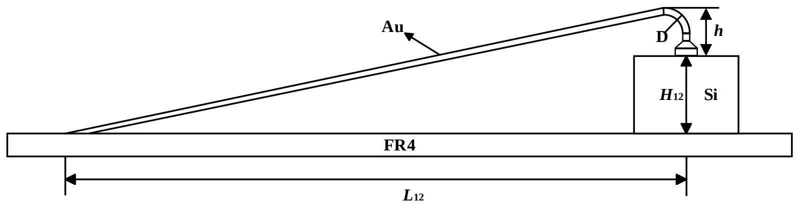

Figure 4: Parametric structural model.

Based on the actual dimensions of the detachable core package, the pressure chip size is 2.5 mm × 2.5 mm × 1.2 mm. The horizontal spacing between the bonding pads on the pressure chip and the PCB, L_{12}, is kept constant at 1.5 mm, the bonding wire diameter D is 25 μm, and the wire loop height h is 150 μm. By varying the thickness of the PCB, the vertical distance between the two bonding points, H_{12}, is adjusted. Four cases are considered, with H_{12} set to 0, 0.2, 0.4, and 0.6 mm, respectively.

3.2. Material Parameters

Table 1 presents the material parameters for each component, chiefly comprising the silicon pressure chip (Si), the gold bonding wire (Au), and the FR4 substrate material of the PCB.

Table 1: Material parameters for gold wire bonding.

Material	Density (kg/m³)	Poisson's ratio	Young's modulus (GPa)	Coefficient of thermal expansion (10^{-6}/K)	Thermal conductivity (W/(m·K))	Specific heat capacity at constant pressure (J/(kg·K))
Au	19300	0.44	70	14.2	317	129
Si	2329	0.28	170	2.6	130	700
FR4	1900	0.15	22	18	0.3	1369

3.3. Temperature Cycling Conditions

The temperature cycling was specified according to Condition G of the JESD22-A104F standard, with upper and lower temperature limits of −40 °C and 125 °C, respectively. The temperature cycling profile is shown in Figure 5. Since the equivalent plastic strain becomes relatively stable after the first four cycles, a total of four temperature cycles were applied. Each temperature cycle consists of four steps, corresponding to the four stages of the thermal cycle:

Stage 1: ramp up from room temperature (25 °C) to the high-temperature state (125 °C) at a heating rate of 16.5 °C/min;

Stage 2: dwell at 125 °C for 15 min;

Stage 3: ramp down from 125 °C to the low-temperature state (−40 °C) at a cooling rate of 16.5 °C/min;

Stage 4: dwell at −40 °C for 15 min.

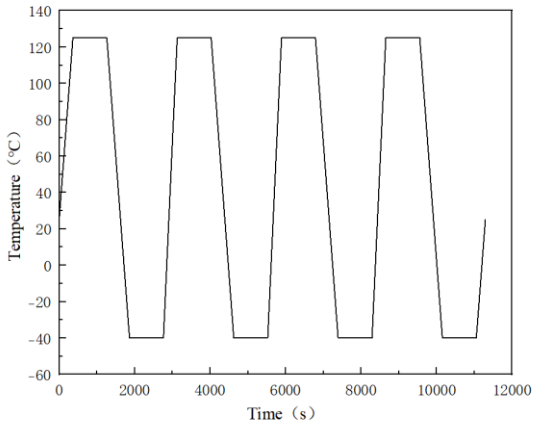

Figure 5: Temperature cycling profile.

4. Results and Analysis

4.1. Equivalent Stress Analysis

The equivalent stress analysis for the case of $H_{12} = 0$ mm yields the following conclusions. Figures 6 and 7 present the transient simulation results. The equivalent stress distribution reveals that the equivalent stress in the gold bonding wire varies periodically with time. The maximum equivalent stress occurs at the neck of the first bond. As the temperature rises, the equivalent stress increases continuously and reaches its maximum value during the high-temperature dwell stage at 125 °C, with a peak stress of 346 MPa. Subsequently, as the temperature decreases, the equivalent stress first declines and then rises, exhibiting another maximum during the low-temperature dwell stage at −40 °C, with a peak stress of 198 MPa.

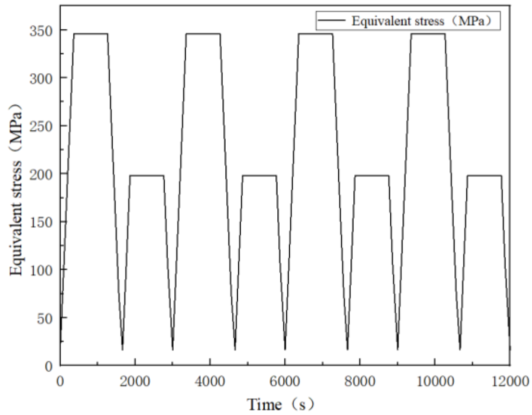

Figure 6: Equivalent stress versus time.

Subsequently, the same loading conditions were applied to the gold bonding wires with the other three height differences. The simulation results indicate that the wires with these three different height differences exhibit characteristics similar to those observed in the $H_{12} = 0$ mm case, although the magnitude of the equivalent stress differs for each height difference. For $H_{12} = 0$ mm, where no vertical height difference exists between the two bonding points, the maximum equivalent stress occurs during the high-temperature dwell stage (125 °C) and reaches 346 MPa. For $H_{12} = 0.6$ mm, the maximum equivalent stress also occurs during the high-temperature dwell stage (125 °C), with a value of 601 MPa. It can therefore be concluded that the maximum equivalent stress increases continuously as H_{12} increases. When H_{12} is reduced from 0.6 mm to 0 mm, the maximum equivalent stress decreases by 42%. Since the silicon piezoresistive pressure chip is extremely sensitive to stress, in order to minimize the equivalent stress exerted on the pressure chip, the configuration with no vertical height difference between the two ends of the bonding wire, i.e., $H_{12} = 0$ mm, is selected.

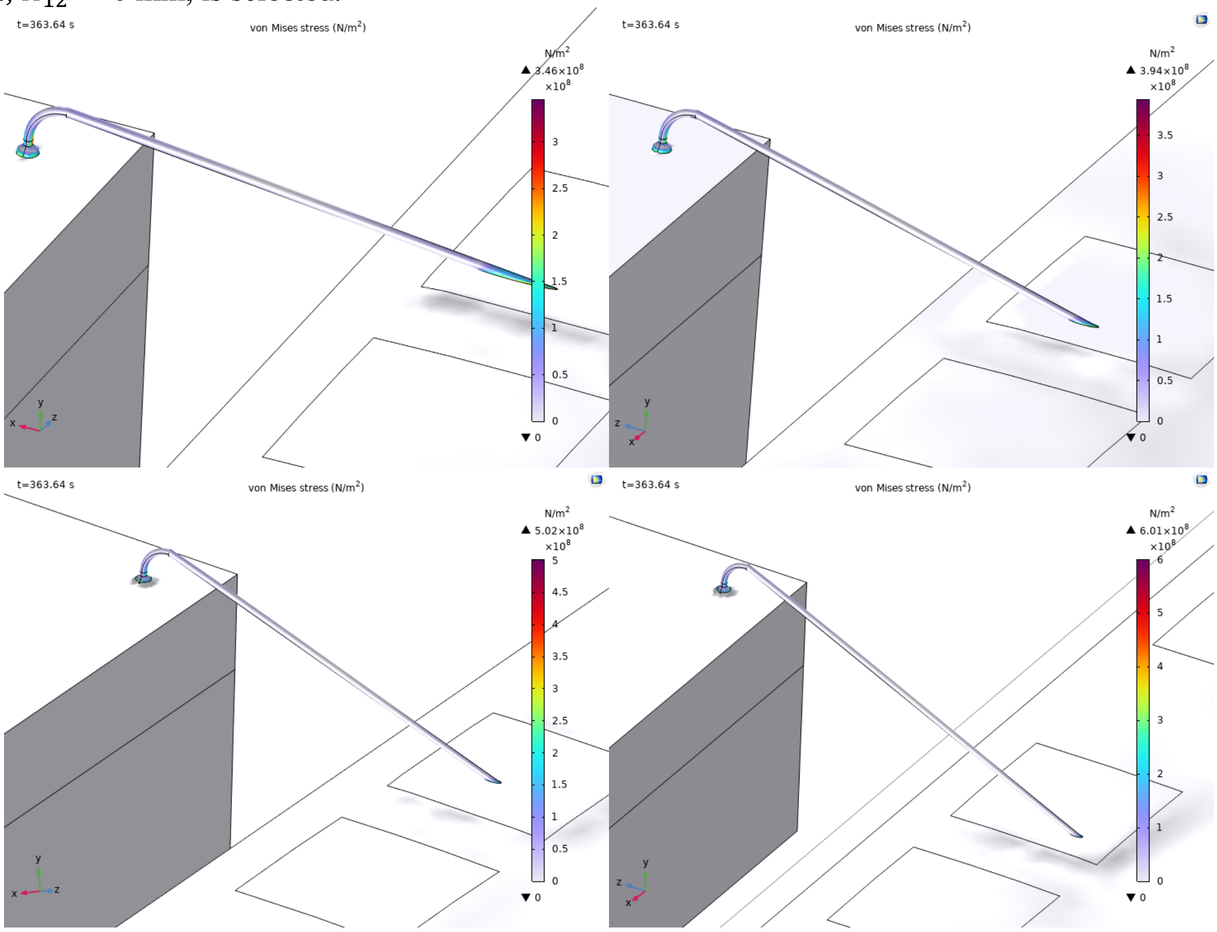

Figure 7: Equivalent stress distribution of the Au wire at different H_{12} values (0, 0.2, 0.4, and 0.6 mm, respectively).

4.2. Deformation Analysis

Since the planar packaging structure of the pressure chip has an unadjustable height difference between the bonding points and the gold wire is prone to horizontal wire sweep or vertical wire sagging, its reliability is relatively low. To address this, a detachable core package structure is proposed, which can alter the vertical distance H_{12} between the two bonding points of the gold wire bond by adjusting the thickness of the PCB. To verify its reliability, the deformation of the gold wire under different height differences between the two bonding points is simulated and analyzed. Taking the case of $H_{12} = 0$ mm as an example, it can be observed from the Figure 8 that when $H_{12} = 0$ mm, the maximum deformation of the gold bonding wire occurs at the midpoint of the wire loop, and the magnitude of deformation varies over time. As the temperature continues to rise, the deformation of the bonding wire increases steadily and reaches a maximum during the high-temperature dwell stage (125 °C), with a peak value of 4.29 μm. During the temperature decrease, the deformation of the bonding wire, similar to the equivalent stress, shows a trend of first decreasing and then increasing, and reaches another maximum during the low-temperature dwell stage (−40 °C), with a peak value of 2.45 μm.

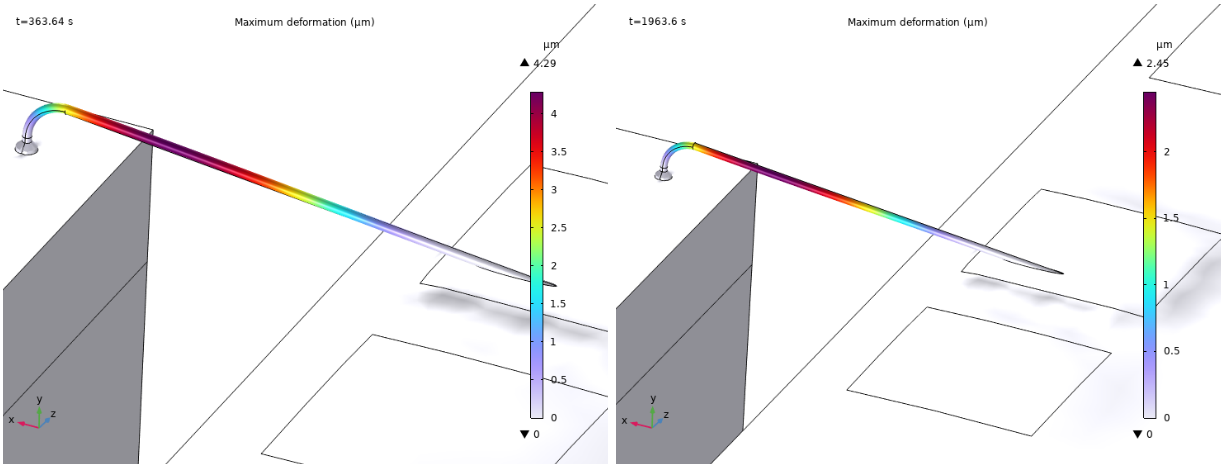

Figure 8: Maximum deformation of the gold bonding wire during the high-temperature (125 ℃) and low-temperature (−40 °C) dwell stages at H_{12} = 0 mm.

Table 2 presents the deformation magnitudes of the gold bonding wires with four different height differences at different temperatures. Under the conditions that the wire diameter D, the horizontal distance between the two bonding points L_{12}, and the wire loop height h remain constant, the deformation of the gold bonding wire exhibits a certain regularity as the vertical distance H_{12} between the two bonding points varies. In the high-temperature state (125 °C), the deformation of the bonding wire increases with increasing H_{12}, and the deformation direction is along the positive Y-axis, i.e., the wire appears in a bulging state. In the low-temperature state (−40 °C), the deformation also increases with increasing H_{12}, but the deformation direction is opposite to that in the high-temperature state—along the negative Y-axis—indicating that the wire appears in a sagging state.

Table 2: Deformation magnitudes of gold bonding wires with four different height differences at different temperatures.

Vertical distance between bonding points H_{12} (mm)	Deformation at 125 °C (μm)	Deformation at 25 °C (μm)	Deformation at −40 °C (μm)
0	4.29	0.204	2.45
0.2	4.68	0.223	2.68
0.4	4.95	0.236	2.83
0.6	6.48	0.309	3.7

Figure 9 presents the relationship between the deformation magnitude and H_{12} under different temperature conditions.

It can be observed from the figure that in the high-temperature state, when the vertical distance H_{12} between the two bonding points is reduced from 0.6 mm to 0 mm, the deformation of the gold bonding wire decreases by 33.796%. In the low-temperature state, the same reduction in H_{12} leads to a decrease of 33.783% in deformation. At room temperature, the deformation is reduced by 33.981% as H_{12} decreases from 0.6 mm to 0 mm. Moreover, when H_{12} is less than 0.4 mm, the curve is relatively flat; when H_{12} exceeds 0.4 mm, the curve becomes steep and the wire undergoes severe deformation.

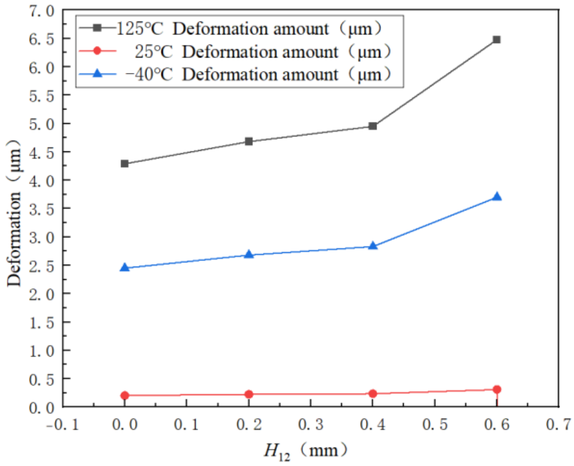

Figure 9: Deformation magnitude versus H_{12} at different temperatures.

4.3. Fatigue Life Prediction

In summary, when there is no vertical height difference between the two bonding points, i.e., $H_{12} = 0$ mm, both the equivalent stress and the deformation of the gold bonding wire are minimized. Therefore, the reliability of the gold wire bond under this condition is analyzed. The reliability of the gold bonding wire is predicted based on the stress and strain results obtained from finite element simulation and a fatigue life model. For instance, in power cycling tests or temperature cycling tests, the fatigue life is typically related to the alternating stress/strain caused by cyclic temperature fluctuations. In general, when the number of cycles exceeds 10^5, it is considered high-cycle fatigue, which is primarily stress-dominated; when the number of cycles is below 10^5, it is low-cycle fatigue, which is primarily strain-dominated.

Whether dealing with high-cycle or low-cycle fatigue, especially for complex components, it is difficult to predict fatigue life through analytical approaches. Consequently, the Coffin–Manson empirical formula is employed to predict the fatigue life of the gold bonding wire [7]. The empirical formula is given as follows:

$$N_f = C_1 \cdot \Delta\varepsilon^{C_2} \tag{1}$$

$$\Delta\varepsilon = \frac{\Delta\varepsilon_1 + \Delta\varepsilon_2 + \Delta\varepsilon_3 + \Delta\varepsilon_4}{4} \tag{2}$$

where $\Delta\varepsilon$ is the plastic strain amplitude, taken as the average value over the four cycles; C_1 and C_2 are two fitting parameters, with $C_1 = 28.38$ and $C_2 = -0.695$; and $\Delta\varepsilon_1$, $\Delta\varepsilon_2$, $\Delta\varepsilon_3$, and $\Delta\varepsilon_4$ are the differences between the maximum and minimum plastic strain amplitudes in each of the four temperature cycles. For the case in which there is no height difference between the two bonding points of the gold wire, the average value of $\Delta\varepsilon$ over the four cycles is 0.0036482143, and the corresponding fatigue life is calculated to be 1404 cycles. This predicted life value indicates that zero-height-difference bonding exhibits an acceptable fatigue life under temperature cycling conditions and can satisfy the reliability requirements of typical engineering environments.

5. Conclusions

This study proposes a detachable core package that permits independent pressure-chip replacement and adjustment of the bonding-point height difference through PCB thickness. Finite element results show that the maximum equivalent stress occurs at the first-bond neck during the high-temperature stage, while the maximum deformation occurs at the wire-loop midpoint. Both increase with H_{12}, particularly above 0.4 mm. Reducing H_{12} from 0.6 to 0 mm decreases the maximum stress by 42% and the high-temperature deformation by 33.8%. Coffin–Manson analysis predicts a fatigue life of 1404 cycles for zero-height-difference bonding, indicating that this configuration meets general engineering reliability requirements. The present study is entirely simulation-based; experimental validation will be conducted in future work.

Acknowledgements

We sincerely acknowledge the support from the Shaanxi Qinchuangyuan "Scientist + Engineer" Team Construction Project 2024QCY-KXJ-192.

References

[1] Wang Huan, Zeng Qinghua. Review of Research Progress on Pressure Scanning Valve Pressure Measurement Systems [J]. Aerospace Metrology Technology, 2021, 41(6): 76-81.

[2] Jiang Yuqi, Liu Shuli, Xia Chenhui, et al. Parametric Modeling and Simulation of Silicon-Aluminum Wire Bonding [J]. Electronics & Packaging, 2022, 22(9): 31-36. DOI: 10.16257/j.cnki.1681-1070.2022.0910.

[3] KUMAR S,RATHORE P K,RANGABABU P. Implementation of operational amplifier for the designing of novel piezoresistive pressure sensor [C]//2018 2nd International Conference on Smart Sensors and Application(ICSSA),2018:126 -129.

[4] Ji Liuxin. Design and Application Research of Miniaturized High-Precision Multi-Channel Pressure Scanning Valve [D]. Jiangnan University, 2024.

[5] Sun Tingxiao, Wu Junjie, Wang Xiwen, et al. Prediction of Bond Wire Fatigue Life and Reliability Analysis for SiP Modules [J]. Research and Progress in Solid State Electronics, 2022, 42(6): 479-483+504. DOI: 10.19623/j.cnki.rpsse.2022.06.001.

[6] Chang Liang, Sun Bin, Xu Pinli, et al. Analysis of the Main Factors Leading to Failure of Gold Wire Bonding [J]. Specialized Equipment for Electronics Industry, 2021, 50(2): 23-28.

[7] Chidambaram N V. A numerical and experimental study of temperature cycle wire bond failure[C]. Electronic Components and Technology Conference, 1991. Proceedings. IEEE Xplore, 1991:877-882.